Advances in Aircraft and Spacecraft Science, *Vol. 12, No. 2 (2025) 161-175*
https://doi.org/10.12989/aas.2025.12.2.161

Effect of spatial translational motion on lengthwise fracture in functionally graded beams

Victor I. Rizov*[1] and Holm Altenbach[2a]

[1]*Department of Technical Mechanics, University of Architecture, Civil Engineering and Geodesy, 1 Chr. Smirnensky Blvd., 1046-Sofia, Bulgaria*
[2]*Lehrstuhl für Technische Mechanik, Fakultät für Maschinenbau, Otto-von-Guericke-Universität Magdeburg, Universitätsplatz 2, 39106 Magdeburg, Deutschland*

(Received April 22, 2025, Revised May 28, 2025, Accepted June 5, 2025)

Abstract. Beam-like structural members and components manufactured by functionally graded materials are widely applied in up-to-date aeronautical and aerospace engineering. Being parts of various flying apparatuses (helicopters, aircrafts, spacecrafts, etc.) these structural members very often are involved in different types of non-uniform spatial motion in the time of their service. This fact indicates the importance of studying the fracture behavior of the structural members and components with taking into account the inertia loading in the conditions of spatial motion. The present paper analyzes the effects of spatial translational motion on lengthwise fracture in functionally graded beams with non-linear elastic behavior. The beams under consideration are executing spatial translational motion with acceleration along the three axes in the space. The law of motion of the beams is known. The paper is focused particularly on deriving the strain energy release rate (SERR) in the beams acted upon by the inertia loading. The content of this paper is presented in the following consequence. First, the SERR problem in beams executing spatial translational motion is treated generally. Determination of accelerations and inertia loads along the three axes of the beam is considered. Then solution of an example is presented in detail. Finally, results illustrating the effects of spatial translational motion, material inhomogeneity and distribution of material density in the beam structure on the SERR are displayed in various graphs. A comparison in terms of the SERR between plane translation and spatial translation motion is presented. In context of this comparison, the effect of thickness to width ratio of the beam is evaluated.

Keywords: functionally graded beam; inertia loading; inhomogeneity; lengthwise fracture; spatial translational motion

1. Introduction

The functionally graded structural materials representing continuously inhomogeneous composites made by mixing of two or more constituent materials currently are known in the international engineering community mainly by their excellent mechanical properties and the ability to operate under heavy loadings and influences (Butcher *et al.* 1999, Gasik 2010, Hamza Hameed *et al.* 2024, Hedia *et al.* 2014, Rizov and Altenbach 2019, Uymaz 2021). The quickly

*Corresponding author, Professor, E-mail: V_RIZOV_FHE@UACG.BG
[a]Professor, E-mail: holm.altenbach@ovgu.de

http://www.techno-press.org/?journal=aas&subpage=7 ISSN: 2287-528X (Print), 2287-5271 (Online)

developing technologies for manufacturing of functionally graded materials offer very good possibilities for continuous improvement of the properties and performance capacities of these materials by tailoring of their microstructure (Hamza Hameed *et al.* 2024, Hirai and Chen 1999, Kashinath Saha and Shubhankar Bhowmick 2020, Mahamood and Akinlabi 2017, Markworth *et al.* 1995, Miyamoto *et al.* 1999, Nemat-Allal *et al.* 2011, Saiyathibrahim *et al.* 2016, Uymaz 2023). The main advantages of functionally graded materials include smooth change of their microstructure which reduces stress concentrations, high specific strength and stiffness, improved fatigue properties, high toughness, improved ability to work at elevated temperatures, etc. (Hamza Hameed and Zaman 2024, Rizov 2020, Shrikantha Rao and Gangadharan 2014, Wu *et al.* 2014, Uymaz 2023, Uymaz and Uymaz 2024). These advantages make the functionally graded materials a desired replacement of the classical homogeneous materials and of the fiber reinforced composites in many segments of the modern engineering including in the aerospace and aeronautics (Mahamood and Akinlabi 2017, Markworth *et al.* 1995, Miyamoto *et al.* 1999, Rizov 2024, Shrikantha Rao and Gangadharan 2014).

The wide range of applications of the functionally graded materials in the current aerospace and aeronautical engineering leads to a constant raising of the requirements towards the safety, reliability and durability of the functionally graded structural members and components under a variety of loadings (including dynamic loading) and environmental influences. The issue of safety is closely related to fracture performance of structures (Dolgov 2002, Dolgov 2005, Dolgov 2016, Dolgov 2024, Dowling 2013, Rizov and Altenbach 2022, Rizov 2025). The beam-like structural members and components made by functionally graded materials being parts of various flying apparatuses frequently are involved in non-uniform spatial motion. Therefore, it is of great practical importance to develop various fracture analyses of functionally graded beam structural components under inertia loadings in the conditions of different kinds of spatial motion.

In particular, the aim of the present paper is to analyze the influence of spatial translational motion on lengthwise fracture in beam structures (the functionally graded beams are prone to lengthwise fracture since very often they are manufactured layer-by-layer which creates premises for appearance of lengthwise cracks (Mahamood and Akinlabi 2017, Rizov 2022). The beams are functionally graded along their length and exhibit non-linear elastic behavior. The motion of the beams is with acceleration along the three axes in the space. Besides, the law of motion is known (it should be noted here that many components of flying apparatuses are designed to execute certain kind of motions in known laws). The acceleration generates inertia loadings on the beam structure along the three axes in the space. The analysis is concerned with deriving the SERR in the beams under inertia loadings. First, the SERR problem in these conditions is treated generally. Then, solution of an example is presented in detail. Various results revealing the influences of spatial translational motion, material inhomogeneity and distribution of density of the material on the SERR are obtained in reported in forms of different graphs. The SERR in a beam executing planar translational motion is compared to that in a beam executing spatial translation.

2. Approach for analysis of lengthwise fracture in functionally graded beams executing spatial translational motion

Consider the rectangular beam structural component displayed in Fig. 1.

Its width, thickness and length are b, h and l, respectively. A lengthwise crack of length, a, splits the beam portion, L_2L_3. The upper and lower arms of the crack have thickness, h_1 and h_2,

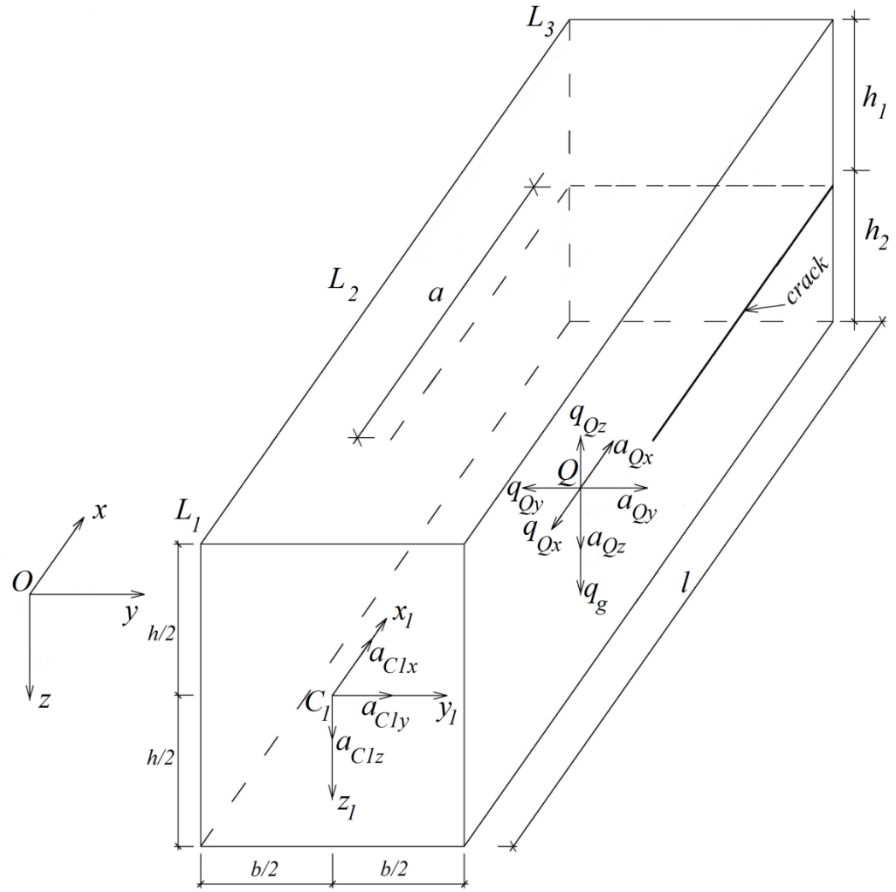

Fig. 1 Schematic diagram of the beam executing spatial translational motion

respectively. The beam executes spatial translational motion. The laws of this motion along the axes, x, y and z, express the coordinates, x_{C1}, y_{C1} and z_{C1}, of the centre, C_1, of the left-hand end of the beam as functions of time, t.

The components, a_{C1x}, a_{C1y} and a_{C1z}, of the acceleration of C_1 are determined as second derivatives of x_{C1}, y_{C1} and z_{C1} with respect to t (Fig. 1).

Since the motion is translational, all the points of the beam have the same acceleration. Thus, the components, a_{Qx}, a_{Qy} and a_{Qz}, of the acceleration of a random point, Q, in the beam are equal to a_{C1x}, a_{C1y} and a_{C1z}, respectively.

The beam is functionally graded along its length. Therefore, the mass density, i.e., the mass per unit length, m_D, changes continuously in longitudinal direction of the beam as written below

$$m_D = f_D(x_1), \tag{1}$$

where

$$0 \le x_1 \le l. \tag{2}$$

Here, f_D is a smooth function of x_1 (the centroidal axis, x_1, is displayed in Fig. 1.

The densities of the inertia loads, q_{Qx}, q_{Qy} and q_{Qz}, along the beam axes in the point, Q, are found by Eqs. (3), (4) and (5), respectively.

$$q_{Qx} = m_D a_{Qx}, \tag{3}$$

$$q_{Qy} = m_D a_{Qy}, \tag{4}$$

$$q_{Qz} = m_D a_{Qz}. \tag{5}$$

The densities, q_{Qx}, q_{Qy} and q_{Qz}, are displayed in Fig. 1.

The density of the deadweight, q_g, of the beam in point, Q, is defined by Eq. (15).

$$q_g = m_D g, \tag{6}$$

where g is the gravity acceleration. The density, q_g, is displayed in Fig. 1.

This study is focused at first place on deriving the SERR, G, in the beam under consideration. Since the beam has non-linear elastic behavior, we use the complementary strain energy, U^*, cumulated in the beam to derive the SERR via Eq. (7).

$$G = \frac{dU^*}{bda}, \tag{7}$$

where da is an infinitesimal increase of the crack length.

In order to determine U^*, we begin with obtaining the complementary strain energy, U^*_{L1L2}, cumulated in the intact portion, L_1L_2, of the beam through Eq. (8).

$$U^*_{L1L2} = \iiint_{(V_{L1L2})} u_0^* dV, \tag{8}$$

where V_{L1L2} is the volume of this beam portion, u_0^* is density of the complementary strain energy. Eq. (9) is applied for deriving u_0^*, i.e.

$$u_0^* = \sigma\varepsilon - \int \sigma d\varepsilon, \tag{9}$$

where σ and ε are the stress and strain, respectively. Since the beam has non-linear elastic behavior, the stress is determined by using a constitutive law of the type written in Eq. (10).

$$\sigma = f_\sigma(\varepsilon), \tag{10}$$

where f_σ is a smooth non-linear function of the strain. Due to the fact that the beam is continuously inhomogeneous along its length, the parameters of the law in Eq. (10) are smooth functions of x_1 where

$$0 \le x_1 \le l. \tag{11}$$

Since the beam is under axial force and bending moments about the horizontal and vertical centric axes of cross-section, the distribution of ε is described by the law in Eq. (12).

$$\varepsilon = \varepsilon_0 + \kappa_{y2} y_2 + \kappa_{z2} z_2, \tag{12}$$

where

$$-\frac{b}{2} \le y_2 \le \frac{b}{2}, \tag{13}$$

$$-\frac{h}{2} \le z_2 \le \frac{h}{2}. \tag{14}$$

Here, y_2 and z_2 are the horizontal and vertical centric axes of a random cross-section of the

intact portion of the beam, ε_0, k_{y2} and κ_{z2} are the strain in the cross-section centre, and the curvatures of the beam in x_2y_2 and x_2z_2 planes, respectively.

The following equations are used for obtaining of ε_0, k_{y2} and κ_{z2}

$$N = \iint_{(A_{L1L2})} \sigma dA, \tag{15}$$

$$M_{y2} = \iint_{(A_{L1L2})} \sigma z_2 dA, \tag{16}$$

$$M_{z2} = \iint_{(A_{L1L2})} \sigma y_2 dA, \tag{17}$$

where N is the axial force, M_{y2} and M_{z2} are the bending moments induced by the inertia loads and the deadweight, σ is expressed by Eq. (10), ε that is involved in Eq. (10) is expressed by Eq. (12). The MatLab is used for solving Eqs. (15), (16) and (17) about unknowns, ε_0, k_{y2} and κ_{z2}.

We continue further with determination of the complementary strain energies, U^*_{upa}, and U^*_{lwa}, in the upper and lower arm of the longitudinal crack. For this purpose, Eqs. (18) and (19) are applied.

$$U^*_{upa} = \iiint_{(V_{upa})} u^*_{0upa} dV, \tag{18}$$

$$U^*_{lwa} = \iiint_{(V_{lwa})} u^*_{0lwa} dV, \tag{19}$$

where V_{upa} and V_{lwa} are the volumes of upper and lower arm, $u^*_{0_{upa}}$ and $u^*_{0_{lwa}}$ are the corresponding complementary strain energy densities. Eqs. (20) and (21) are used to determine $u^*_{0_{upa}}$ and $u^*_{0_{lwa}}$, i.e.

$$u^*_{0upa} = \sigma_{upa}\varepsilon_{upa} - \int \sigma_{upa} d\varepsilon_{upa}, \tag{20}$$

$$u^*_{0lwa} = \sigma_{lwa}\varepsilon_{lwa} - \int \sigma_{lwa} d\varepsilon_{lwa}. \tag{21}$$

The stresses, σ_{upa} and σ_{lwa}, are expressed by the strains, ε_{upa} and ε_{lwa}, through the law in Eq. (10). The strains are treated by using Eqs. (22) and (23).

$$\varepsilon_{upa} = \varepsilon_{0upa} + \kappa_{y3} y_3 + \kappa_{z3} z_3, \tag{22}$$

$$\varepsilon_{lwa} = \varepsilon_{0lwa} + \kappa_{y4} y_4 + \kappa_{z4} z_4, \tag{23}$$

where

$$-\frac{b}{2} \le y_3 \le \frac{b}{2}, \tag{24}$$

$$-\frac{h_1}{2} \le z_3 \le \frac{h_1}{2}. \tag{25}$$

$$-\frac{b}{2} \le y_4 \le \frac{b}{2}, \tag{26}$$

$$-\frac{h_2}{2} \le z_4 \le \frac{h_2}{2}. \tag{27}$$

Here, y_3 and z_3 are the centric axes of a random cross-section of the upper arm, ε_{0upa}, k_{y3} and κ_{z3} are the strain in the centre, and the curvatures, y_4 and z_4 are the centric axes of a random cross-section of the lower arm, ε_{0lwa}, k_{y4} and κ_{z4} are the strain in the centre, and the curvatures of the lower arm of the crack. Eqs. (28) and (29) are applied to obtain ε_{0upa}, k_{y3} and κ_{z3}.

$$N_{upa} = \iint_{(A_{upa})} \sigma_{upa} dA, \tag{28}$$

$$M_i = \iint_{(A_{upa})} \sigma_{upa} j dA, \tag{29}$$

where $i = y_3,\ z_3$ and $j = z_3,\ y_3$. Here, N_{upa} is the axial force, M_{i3} are the bending moments in the considered cross-section of the upper arm of the crack. The unknowns, ε_{0lwa}, k_{y4} and κ_{z4}, are found by Eqs. (30) and (31).

$$N_{lwa} = \iint_{(A_{lwa})} \sigma_{lwa} dA, \tag{30}$$

$$M_r = \iint_{(A_{lwa})} \sigma_{lwa} s dA. \tag{31}$$

In Eq. (31), $r = y_4,\ z_4$ and $s = z_4,\ y_4$. Here, N_{lwa} and M_r are the axial force and the bending moments in the considered cross-section of the crack lower arm.

The complementary strain energy in the beam is derived by Eq. (32).

$$U^* = U^*_{L1L2} + U^*_{upa} + U^*_{lwa}, \tag{32}$$

where the integration is carried-out by the MatLab. Finally, the SERR is found by substituting of Eq. (32) in Eq. (7).

3. Example

Solution of an example is reported in this section of the paper with purpose to demonstrate the applicability of the approach presented in section 2. The solution is obtained by using the function, f_σ, (refer to Eq. (10)) written in Eq. (33) (Kishkilov and Apostolov 1994).

$$f_\sigma = \frac{E\varepsilon}{\sqrt{1+n\vec{\varepsilon}\varepsilon^2}}, \tag{33}$$

where E and n are material parameters. In fact, Eq. (33) represents the constitutive law. The change of E and n due to material inhomogeneity along the beam length is described by Eqs. (34) and (35), respectively.

$$E = E_{le} e^{\eta_1 \frac{x_1}{l}}, \tag{34}$$

$$n = n_{le} e^{\eta_2 \frac{x_1}{l}}, \tag{35}$$

where

$$0 \le x_1 \le l. \tag{36}$$

Here, E_{le} and n_{le} are the values of E and n in the left-hand end of the beam, η_1 and η_2 are parameters.

The function, f_D, that describes the change of the mass density along the beam length (refer to Eq. (1)) is given below.

$$f_D = m_{Dle} e^{\eta_3 \frac{x_1}{l}}, \tag{37}$$

where m_{Dle} is the mass density in the left-hand of the beam, η_3 is parameter. Here, again

$$0 \le x_1 \le l. \tag{38}$$

The laws of spatial translational motion of the beam structure are written in the next three equations, i.e.

$$x_{C1} = \mu_1 t^{\mu_2}, \tag{39}$$

$$y_{C1} = \mu_3(e^{\mu_4 t} - 1), \tag{40}$$

$$z_{C1} = \mu_5^{\mu_6 t} - 1, \tag{41}$$

where $\mu_1,\ \mu_2,\ \ldots, \mu_6$ are parameters. From Eqs. (39), (40) and (41) it follows that

$$a_{Qx} = \mu_1\mu_2(\mu_2 - 1)t^{\mu_2 - 2}, \tag{42}$$

$$a_{Qy} = \mu_3\mu_4^2 e^{\mu_4 t}, \tag{43}$$

$$a_{Qz} = \mu_5^{\mu_6 t}(ln\,\mu_5)^2\mu_6^2. \tag{44}$$

The densities of the inertia loads are found by substituting of Eqs. (37), (42), (43) and (44) in Eqs. (2), (3) and (4). The result is given below.

$$q_{Qx} = m_{Dle} e^{\eta_3 \frac{x_1}{l}} \mu_1\mu_2(\mu_2 - 1)t^{\mu_2 - 2}, \tag{45}$$

$$q_{Qy} = m_{Dle} e^{\eta_3 \frac{x_1}{l}} \mu_3\mu_4^2 e^{\mu_4 t}, \tag{46}$$

$$q_{Qz} = m_{Dle} e^{\eta_3 \frac{x_1}{l}} \mu_5^{\mu_6 t}(ln\,\mu_5)^2\mu_6^2. \tag{47}$$

Further, we determine N, M_{y2} and M_{z2} in a random cross-section of the intact beam portion. The distance between this cross-section and the left-hand end of the beam is denoted by ω. It should be specified that ω may take values between 0 and $l - a$. To determine N, M_{y2} and M_{z2}, we perform reduction of the inertia loads and the deadweight that act upon the part of the beam rightward of the cross-section under consideration. In this way, we obtain

$$N = \int_{\omega}^{l} q_{Qx}\, dx_1, \tag{48}$$

$$M_{y2} = \int_{\omega}^{l} (q_g - q_{Qz})(x_1 - \omega)\, dx_1, \tag{49}$$

$$M_{z2} = \int_{\omega}^{l} q_{Qy}(x_1 - \omega)\, dx_1. \tag{50}$$

The so determined N, M_{y2} and M_{z2} are used to derive ε_0, k_{y2} and κ_{z2} by Eqs. (15), (16) and (17) with the help of the MatLab.

The quantities, N_{upa}, M_{y3} and M_{z3}, in a random cross-section are determined by carrying-out reduction of the inertia loads and deadweight acting upon the part of the upper arm of the crack located rightward of the cross-section under consideration. The distance between the cross-section and the left-hand end of the beam is ω_{upa} where ω_{upa} may vary between $l - a$ and l. The reduction is written in Eqs. (51), (52) and (53).

$$N_{upa} = \int_{\omega_{upa}}^{l} q_{Qxupa}\, dx_1, \tag{51}$$

$$M_{y3} = \int_{\omega_{upa}}^{l} (q_{gupa} - q_{Qzupa})\big(x_1 - \omega_{upa}\big)\, dx_1, \tag{52}$$

$$M_{z3} = \int_{\omega_{upa}}^{l} q_{Qyupa}\big(x_1 - \omega_{upa}\big)\, dx_1, \tag{53}$$

where

$$q_{Qxupa} = q_{Qx}\frac{h_1}{h}, \tag{54}$$

$$q_{Qyupa} = q_{Qy}\frac{h_1}{h}, \tag{55}$$

$$q_{Qzupa} = q_{Qz}\frac{h_1}{h}, \tag{56}$$

$$q_{gupa} = q_g\frac{h_1}{h}. \tag{57}$$

Then N_{upa}, M_{y3} and M_{z3} are used for deriving ε_{0upa}, k_{y3} and κ_{z3} through Eqs. (28) and (29) by the MatLab.

Next, we obtain N_{lwa}, M_{y4} and M_{z4} by performing reduction of the inertia loads and deadweight that act upon the part of the lower arm of the crack located rightward of a random cross-section (the distance between the cross-section and the left-hand end of the beam is ω_{lwa}). The reduction is given below.

$$N_{lwa} = \int_{\omega_{lwa}}^{l} q_{Qxlwa}\, dx_1, \tag{58}$$

$$M_{y4} = \int_{\omega_{lwa}}^{l} (q_{glwa} - q_{Qzlwa})(x_1 - \omega_{lwa})\, dx_1, \tag{59}$$

$$M_{z4} = \int_{\omega_{lwa}}^{l} q_{Qylwa}(x_1 - \omega_{lwa})\, dx_1, \tag{60}$$

where

$$q_{Qxlwa} = q_{Qx}\frac{h_2}{h}, \tag{61}$$

$$q_{Qylwa} = q_{Qy}\frac{h_2}{h}, \tag{62}$$

$$q_{Qzlwa} = q_{Qz}\frac{h_2}{h}, \tag{63}$$

$$q_{glwa} = q_g\frac{h_2}{h}. \tag{64}$$

The quantities, N_{lwa}, M_{y4} and M_{z4}, determined by Eqs. (58), (59) and (60) are used to derive ε_{0lwa}, k_{y4} and κ_{z4} by Eqs. (30) and (31).

At the end, the SERR is found by substituting of U^* (obtained by Eq. (42)) in Eq. (7).

The so found SERR is confirmed by applying the solution reported in (Rizov 2020). The expression of the SERR obtained in (Rizov 2020) is given below.

$$G = \frac{1}{b}\Big(\iint_{(A_{upa})} u^*_{0upa} dA + \iint_{(A_{lwa})} u^*_{olwa} dA - \iint_{(A_{L1L2})} u^*_0 dA \Big), \tag{65}$$

where u^*_{0upa} and u^*_{0lwa} are the complementary strain energy densities in the upper and lower arms of the crack behind the crack tip, u^*_0 is the complementary strain energy density in the beam ahead of the crack tip. The results yielded by Eq. (65) match these determined by Eq. (7) which confirms that the present analysis is correct.

We continue further with studying how the longitudinal fracture in the beam structure executing spatial translational motion is affected by a variety of parameters. In this relation we apply the solution of the SERR for performing a parametric analysis. The following data are used:

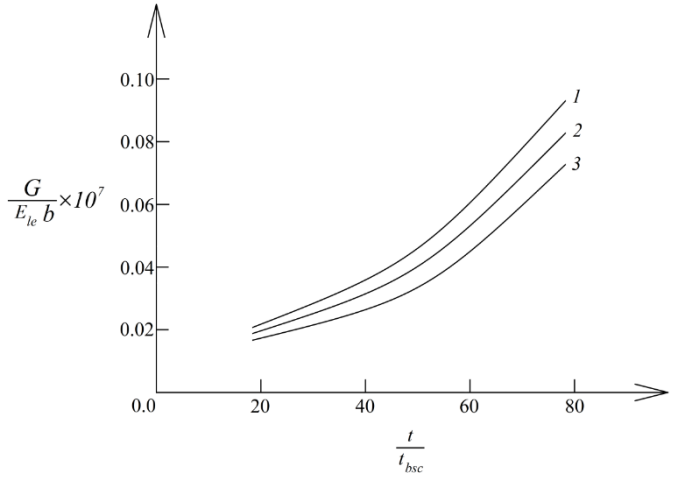

Fig. 2 Change of the SERR with time (graph 1-at $\eta_1 = 0.2$, graph 2-at $\eta_1 = 0.5$ and graph 3-at $\eta_1 = 0.8$)

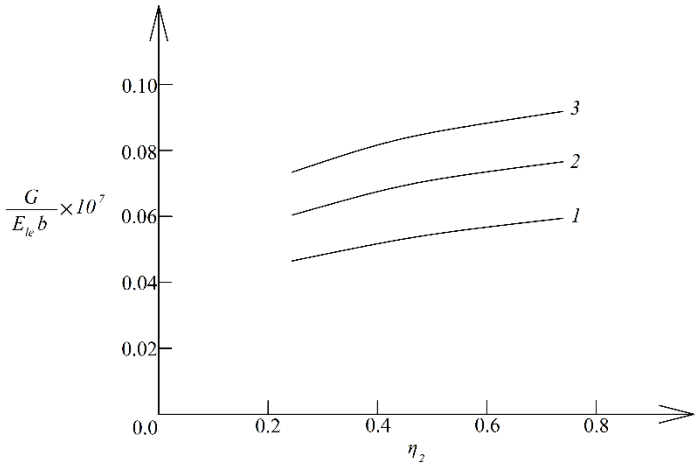

Fig. 3 Change of the SERR with η_2 (graph 1-at $\eta_3 = 0.3$, graph 2-at $\eta_3 = 0.6$ and graph 3-at $\eta_3 = 0.9$)

$b = 0.040$ m, $h = 0.060$ m, $l = 0.750$ m, $a = 0.550$ m and $h_1 = 0.030$ m.

Since the inertia loads depend on time, the longitudinal fracture in the translatory moving beam under consideration also depends on time. Hence, it is important to examine this dependency. For this purpose, the change of the SERR with time under action of the inertia loads is analyzed. The graphs displayed in Fig. 2 illustrate this change (the SERR in Fig. 2 is reported in non-dimensional form by applying the formula $G/(E_{le}b)$). One can see in Fig. 2 that the SERR rapidly grows with time (this observation is attributed to the increase of the magnitudes of the inertia loads with time). The change of the SERR induced by the growth of parameter, η_1, is also examined. The influence of η_1 is illustrated in Fig. 2 where the SERR-time graphs obtained at different magnitudes of η_1 are displayed. It can be seen that the SERR reduces with rise of η_1.

It is studied also how the SERR is affected by rise of the magnitudes of parameters, η_2 and η_3. The change of the SERR when both η_2 and η_3 are varied is illustrated by the graphs reported in Fig. 3.

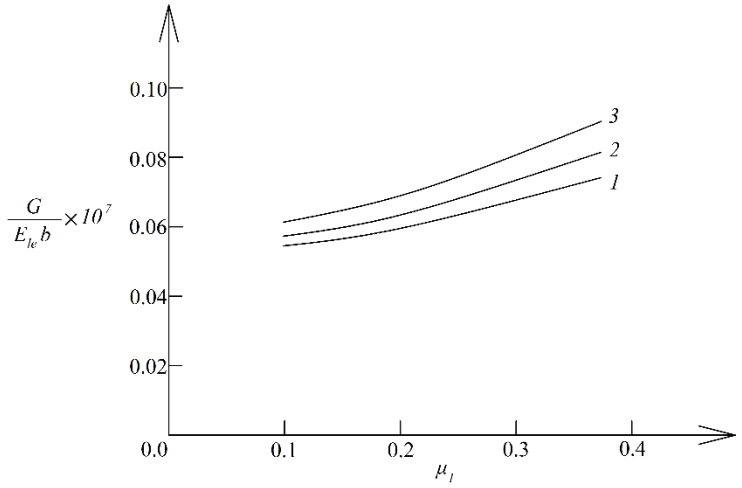

Fig. 4 Change of the SERR with μ_1 (graph 1-at $\mu_2 = 2.5$, graph 2-at $\mu_2 = 3.0$ and graph 3-at $\mu_2 = 3.5$)

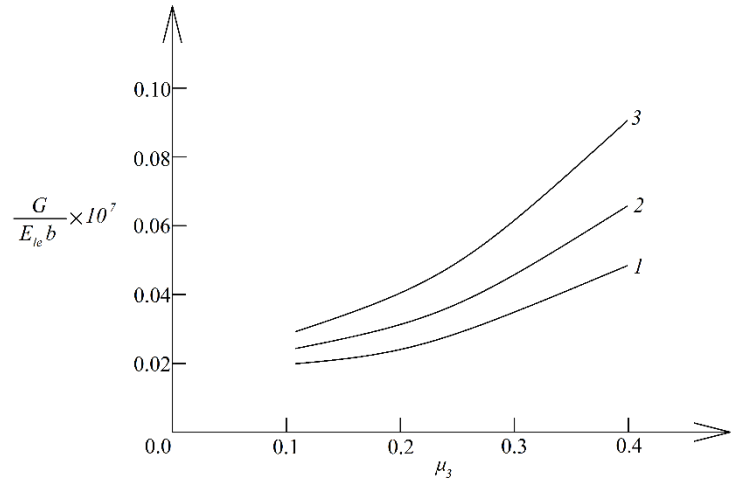

Fig. 5 Change of the SERR with μ_3 (graph 1-at $\mu_4 = 0.05$, graph 2-at $\mu_4 = 0.10$ and graph 3-at $\mu_4 = 0.15$)

As one can observe in Fig. 3 the slope of the SERR-η_2 graphs is relatively small (this means that the SERR slightly increases with rise of the magnitude of η_2).

The increase of the SERR due to rise of η_3 is more considerable (Fig. 3).

It is important to examine how the longitudinal fracture is influenced by the transitional motion of the beam structure. In this relation we analyze the change of the SERR induced by variation of the parameters of the motion.

The influence of the parameters, μ_1 and μ_2, is examined first (these parameters control the translation along the longitudinal axis of the beam). The change of the SERR induced by varying μ_1 and μ_2 is presented in Fig. 4. The inspection of the graphs depicted in Fig. 4 reveals that the SERR grows as a result of rise of the magnitudes of μ_1 and μ_2. It can also be seen in Fig. 4 that the influence of μ_1 and μ_2 on the SERR is relatively modest since the slope of the graphs is small. Besides, the graphs are quite close (Fig. 4).

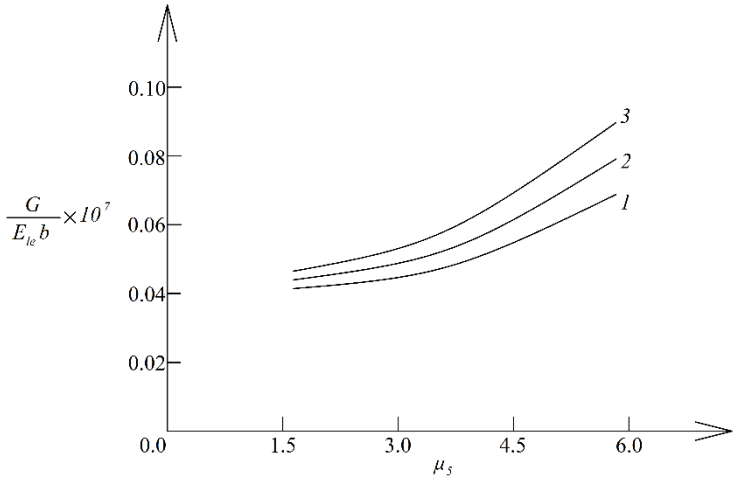

Fig. 6 Change of the SERR with μ_5 (graph 1-at $\mu_6 = 0.05$, graph 2-at $\mu_6 = 0.10$ and graph 3-at $\mu_6 = 0.15$)

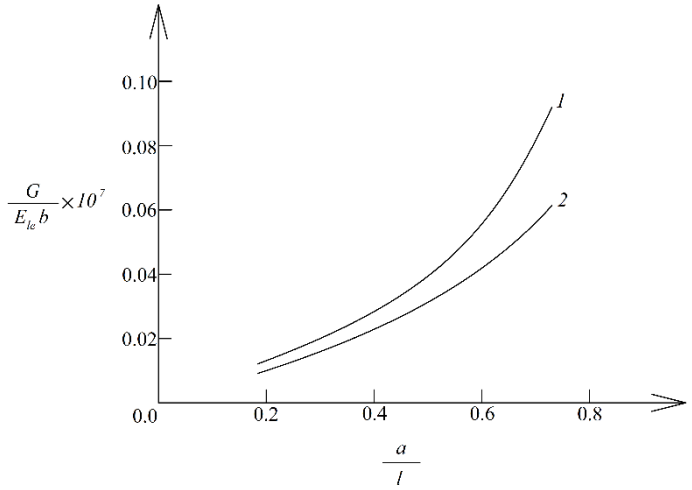

Fig. 7 Change of the SERR with a/l ratio (graph 1-at spatial translational motion of the beam, curve 2-at translational motion of the beam only in plane, x_1z_1)

One can observe how the SERR is affected by the translational motion along the axis, y, in Fig. 5 where SERR- μ_3 graphs obtained at three magnitudes of the parameter, μ_4, are reported. The effect of μ_3 is significant since the SERR rapidly grows with rise of this parameter. The rise of μ_4 also induces substantial growth of the SERR (Fig. 5).

The graphs reported in Fig. 6 give an idea how the parameters, μ_5 and μ_6, influence the SERR (μ_5 and μ_6 govern the beam translational motion in vertical direction). The increase of magnitudes of μ_5 and μ_6 induces growth of the SERR (Fig. 6).

It is useful to evaluate the effect of the spatial translational motion on the longitudinal fracture by comparing with results obtained for the case when the beam executes planar translation in the x_1z_1-plane (Fig. 1). For this purpose, the graph of the dependency of the SERR on a/l ratio obtained at spatial translational motion of the beam is reported in Fig. 7 jointly with analogical

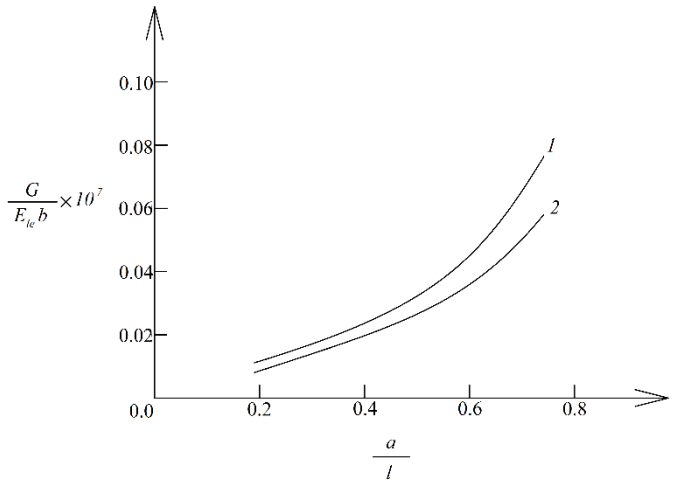

Fig. 8 Change of the SERR with a/l ratio in beam structure with width of 0.060 m and thickness of 0.060 m (graph 1-at spatial translational motion of the beam, curve 2-at translational motion of the beam only in plane, x_1z_1)

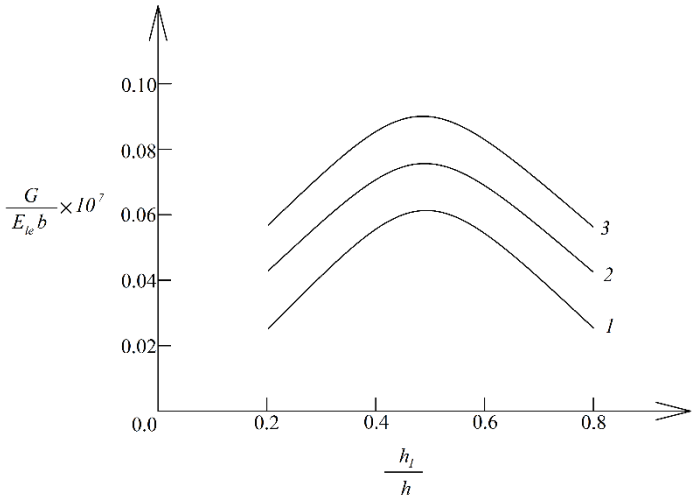

Fig. 9 Change of the SERR with h_1/h ratio (graph 1-at $l/h = 4$, graph 2-at $l/h = 8$ and graph 3- at $l/h = 12$)

graph for the same beam executing planar translation only in the x_1z_1 plane. The solution of the SERR for planar translation is found by inserting $\mu_3 = 0$ in the solution for spatial translation (at $\mu_3 = 0$ the beam structure does not move along the axis, y). The graphs in Fig. 7 indicate that the SERR at spatial translation is higher than the SERR at planar translation. It can be seen also that the SERR grows as result of increase of a/l ratio (Fig. 7).

The graphs in Fig. 7 are obtained for beam structure with width of 0.040 m and thickness of 0.060 m. It is interesting to assess the effect of spatial transitional motion of the beam on the SERR when the width is changed to 0.060 m (the beam thickness is kept unchanged i.e., $h =$ 0.060 m). Graphs of dependency of the SERR on a/l ratio for beam of width, 0.060 m, and

thickness, 0.060 m, are reported for both cases (spatial translation and translation only in the x_1z_1 plane) in Fig. 8. The graphs reveal that the SERR at spatial translation is higher than the SERR at planar translation (Fig. 8). Inspection of Fig. 7 and Fig. 8 indicates that change of the beam width from 0.040 m to 0.060 m leads to reduction of the difference between the SERR at spatial and plane transitional motion. This finding can be explained by increase of the beam stiffness in x_1y_1 plane. As a result of this the SERR due to beam bending in the x_1y_1 plane by the inertia load induced by the beam translation along the axis, y_1, reduces. In other words, when the width of the beam is bigger, the difference between the SERR at spatial and planar translation is smaller.

The graphs displayed in Fig. 9 are obtained by studying the effect of the crack location along the beam thickness on the SERR at spatial translation motion (the ratio, h_1/h, characterizes the crack location). One can observe in Fig. 9 that the SEER has maximum at $h_1/h = 0.5$, i.e., when the crack is the beam mid-plane. Another conclusion that can be made from the graphs in Fig. 9 is that the SERR grows when a/l ratio increases.

5. Conclusions

The main conclusions of this study are as follows:

(1) The SERR rapidly grows with time as a result of increase of the magnitude of the inertial loads induced by spatial translational motion of the beam.

(2) The SERR reduces with increase of the magnitude of the parameter, η_1.

(3) The SERR slightly increases with rise of the magnitude of the parameter, η_2.

(4) Significant increase of the SERR is observed with increase of the magnitude of the parameter, η_2.

(5) The effect of the parameters, μ_1 and μ_2, on the SERR is relatively modest.

(6) The SERR rapidly grows with increase of the magnitudes of the parameters, μ_3 and μ_4.

(7) The increase of the magnitudes of the parameters, μ_5 and μ_6, also induces growth of the SERR.

(8) The SERR at spatial translation is higher than the SERR at planar translation.

(9) Increasing the beam width leads to reducing the difference between the SERR at spatial and planar translational motion.

(10) The SEER has maximum when the longitudinal crack is the beam mid-plane.

Concerning the non-linear constitutive law, the laws for translational motion of the beam, and the laws for change of the parameters, E, n and m_D, along the beam length applied when solving the example in section 3 of the paper it should be specified that these laws are used only to demonstrate the way for application of the general approach. Other laws relevant for a particular case can also be applied.

Acknowledgments

The first author (V. I. R.) acknowledges the German Academic Exchange Organization (DAAD) for the financial support of his research stay in Department of Engineering Mechanics, Institute of Mechanics, Otto-von-Guericke-University, Magdeburg, Germany.

References

Butcher, R.J., Rousseau, C.E. and Tippur, H.V. (1999), "A functionally graded particulate composite: measurements and failure analysis", *Acta. Mater.*, **47**(2), 259-268. https://doi.org/10.1016/S1359-6454(98)00305-X.

Dolgov, M.A. (2024), "Analysis of the stress state in the deformed coating under base stretching with the bending effect account", *Strength Mater.*, **56**, 1127-1135. https://doi.org/10.1007/s11223-025-00723-2.

Dolgov, N.A. (2002), "Effect of the elastic modulus of a coating on the serviceability of the substrate-coating system", *Strength Mater.*, **34**, 153-157. https://doi.org/10.1023/A:1015362426688.

Dolgov, N.A. (2005), "Determination of stresses in a Two-layer coating", *Strength Mater.*, **37**(2), 422-431. https://doi.org/10.1007/s11223-005-0053-7.

Dolgov, N.A. (2016), "Analytical methods to determine the stress state in the substrate-coating system under mechanical loads", *Strength Mater.*, **48**(1), 658-667. https://doi.org/10.1007/s11223-016-9809-5.

Dowling, N.E. (2013), *Mechanical Behaviour of Materials*, Person.

Gasik, M.M. (2010), "Functionally graded materials: Bulk processing techniques", *Int. J. Mater. Prod. Technol.*, **39**(1-2), 20-29. https://doi.org/10.1504/IJMPT.2010.034257.

Hameed, H. and Zaman, F.D. (2024), "Effect of quartic nonlinearity on elastic waves via successive approximation", *Adv. Mater. Res.*, **13**(4), 285-297. https://doi.org/10.12989/amr.2024.13.4.285.

Hameed, H., Munir, S. and Zaman, F.D. (2024), "Green's function coupled with perturbation approach to dynamic analysis of inhomogeneous beams with eigenfrequency and rotational effect's investigations", *Struct. Monit. Mainten.*, **11**(1), 19-40. https://doi.org/10.12989/smm.2024.11.1.019.

Hameed, H., Zaman, F.D., Ahmad, S. and Ali, H. (2024), "Novel results from quadratically nonlinear elastic wave models using Murnaghan's potential", *Arab. J. Math.*, **13**(3), 533-548. https://doi.org/10.1007/s40065-024-00479-8.

Hedia, H.S., Aldousari, S.M., Abdellatif, A.K. and Fouda, N.A. (2014), "New design of cemented stem using functionally graded materials *(FGM)*", *Biomed. Mater. Eng.*, **24**(3), 1575-1588. https://doi.org/10.3233/BME-140962.

Hirai, T. and Chen, L. (1999), "Recent and prospective development of functionally graded materials in Japan", *Mater Sci. Forum*, **308-311**(4), 509-514. https://doi.org/10.4028/www.scientific.net/MSF.308-311.509.

Kishkilov, M. and Apostolov, R. (1994), *Introduction to Theory of Plasticity*, UACEG.

Madan, R., Saha, K. and Bhowmick, S. (2020), "Limit speeds and stresses in power law functionally graded rotating disks", *Adv. Mater. Res.*, **9**(2), 115-131. https://doi.org/10.12989/amr.2020.9.2.115.

Mahamood, R.M. and Akinlabi, E.T. (2017), *Functionally Graded Materials*, Springer.

Markworth, A.J., Ramesh, K.S. and Parks, Jr. W.P. (1995), "Review: Modeling studies applied to functionally graded materials", *J. Mater. Sci.*, **30**(3), 2183-2193. https://doi.org/10.1007/BF01184560.

Miyamoto, Y., Kaysser, W.A., Rabin, B.H., Kawasaki, A. and Ford, R.G. (1999), *Functionally Graded Materials: Design, Processing and Applications*, Kluwer Academic Publishers, Dordrecht/London/Boston.

Nemat-Allal, M.M., Ata, M.H., Bayoumi, M.R. and Khair-Eldeen, W. (2011), "Powder metallurgical fabrication and microstructural investigations of Aluminum/Steel functionally graded material", *Mater. Sci. Appl.*, **2**(5), 1708-1718. https://doi.org/10.4236/msa.2011.212228.

Rizov, V. and Altenbach, H. (2020), "Longitudinal fracture analysis of inhomogeneous beams with continuously varying sizes of the cross-section along the beam length", *Frattura ed Integrità Strutturale*, **53**, 38-50. https://doi.org/10.3221/IGF-ESIS.53.04.

Rizov, V.I. (2020), "Longitudinal fracture analysis of inhomogeneous beams with continuously changing radius of cross-section along the beam length", *Strength Fract. Complex.*, **13**, 31-43. https://doi.org/10.3233/SFC-200250.

Rizov, V.I. (2022), "Analysis of the strain energy release rate for time-dependent delamination in multilayered beams with creep", *Adv. Mater. Res.*, **11**, 41-57. https://doi.org/10.12989/amr.2022.11.1.041.

Rizov, V.I. (2024), "The effect of delamination between layers in U-shaped members made of functionally graded multilayered viscoelastic materials", *J. Appl. Comput. Mech.*, **10**, 830-841. https://doi.org/10.22055/jacm.2024.46014.4449.

Rizov, V.I. (2025), "Longitudinal fracture analysis of continuously inhomogeneous beams undergoing general planar motion", *J. Appl. Comput. Mech.*, 1-13. https://doi.org/10.22055/jacm.2025.48102.4977.

Rizov, V.I. and Altenbach, H. (2019), "On the analysis of lengthwise fracture of functionally graded round bars", *Struct. Integr. Life*, **19**(2), 102-108.

Saiyathibrahim, A., Subramaniyan, R. and Dhanapl, P. (2016), "Centrefugally cast functionally graded materials-Review", *International Conference on Systems, Science, Control, Communications, Engineering and Technology*, 68-73.

Shrikantha Rao, S. and Gangadharan, K.V. (2014), "Functionally graded composite materials: An overview", *Procedia Mater. Sci.*, **5**(1), 1291-1299. https://doi.org/10.1016/j.mspro.2014.07.442.

Uymaz, B. (2021), "Buckling characteristics of FGM plates subjected to linearly varying in-plane loads", *Mech. Compos. Mater.*, **57**, 69-80. https://doi.org/10.1007/s11029-021-09934-5.

Uymaz, B. (2023), "Analytical solution of bending, buckling, and vibration of functionally graded nanobeams based on nonlocal elasticity", *J. Balkan Sci. Technol.*, **2**(1), 37-47 http://doi.org/10.55848/jbst.2023.29.

Uymaz, B. (2023), "Vibration of CFFF functionally graded plates with an attached point mass at an arbitrary point in thermal environment", *J. Vib. Eng. Technol.*, **11**, 1867-1888. https://doi.org/10.1007/s42417-022-00676-9.

Uymaz, B. and Uymaz, G. (2024), "Three-dimensional thermal vibration of CFFF functionally graded carbon nanotube-reinforced composite plates", *J. Vib. Eng. Technol*., **12**, 5345-5368. https://doi.org/10.1007/s42417-023-00957-x.

Wu, X.L., Jiang, P., Chen, L., Zhang, J.F., Yuan, F.P. and Zhu, Y.T. (2014), "Synergetic strengthening by gradient structure", *Mater. Res. Lett.*, **2**(1), 185-191. https://doi.org/10.1080/21663831.2014.935821.

CC